Characteristics of Surface Currents in a Shallow Lagoon–Inlet–Coastal Ocean System Revealed by Surface Drifter Observations

Katherine Fitzenreiter[1] · Miaohua Mao[1,2,3] · Meng Xia[1]

Abstract

The circulation in a shallow lagoon–inlet–coastal ocean system is significant to material transports (e.g., debris, pollutants, and larvae). To study surface flows in this system, we deployed 35 surface drifters at various tidal phases and wind conditions during 2017 and 2018 in the Maryland Coastal Bays system (MCBs). Given that winds and tides are two important drivers of estuarine and coastal circulation, their influences on surface drifter trajectories were analyzed. Observations indicate that surface drifters exit (enter) the lagoon mostly during ebb (flood) currents, and clockwise circular movements at a length scale of 1.5 km formed at the outer edge of Ocean City Inlet (OCI). Under weak wind conditions, tides are primarily responsible for drifter movements near OCI, whereas both the long-fetch winds and tides are important near the relatively larger Chincoteague Inlet and backbays. Under strong wind conditions, surface drifter movements generally follow wind directions. In the shallow lagoonal system, relative effects of winds on surface drifters gradually become stronger in the regions further away from the adjacent inlet as tides are weaker. Further investigations indicate that the fastest and slowest surface drifters are near the small OCI and backbays with the weakened tides, respectively. The direct surface drifter observations that cover a wide spatial range and long time series can provide strong support to surface current simulations. Enhanced understanding of coastal physical oceanography in the MCBs can be beneficial to similar systems and coastal ocean communities.

Introduction

Water currents are crucial in driving particle transport and material exchanges (e.g., nutrients, sediments, and chemicals traveling in the water column) between lagoonal bays and the adjacent coastal ocean, affecting plume dynamics, estuarine health, and coastal ecology (Wazniak et al. 2005; Xia et al. 2007, 2010, 2011). Larval recruitments of fish and

shellfish partly depend on advective transporting by water currents to suitable nursery habitats for the next developing stages (Norcross and Shaw 1984; Jenkins et al. 1997; Brown et al. 2000). Moreover, a clear understanding of the surface circulation patterns, under the combined effects of winds and tides at timescales ranging from several days to months, is fundamental to predicting the advection and dispersion of oil spills from source locations (Reed et al. 1994; Turrell 1994; Annika et al. 2001), carrying out search-and-rescue missions (U.S. Coast Guard 2013), and managing beach nourishment projects (Cipriani and Stone 2001; Krafft 2017).

Surface water currents were previously studied by tracking floating bottles and drifting cards (Harrington 1894). During the second half of the twentieth century, satellite- and GPS (global positioning system)-based surface drifters were developed to derive surface flows (Kjellsson and Döös 2012; Lumpkin et al. 2017). Due to their extensive spatial coverage, surface drifters have been largely employed to reveal surface circulation patterns and features at the global scale (Molcard et al. 2003), mesoscale (10–100 km) (McNally 1981), and sub-mesoscale (1–10 km)

✉ Miaohua Mao
  mhmao@yic.ac.cn

[1] Department of Natural Sciences, University of Maryland Eastern Shore, Princess Anne, Somerset, MD 21853, USA

[2] CAS Key Laboratory of Coastal Environmental Processes and Ecological Remediation, Yantai Institute of Coastal Zone Research, Chinese Academy of Sciences, Yantai, Shandong, P.R. China 264003

[3] Shandong Key Laboratory of Coastal Environmental Processes, Yantai, Shandong, P.R. China 264003

(Spydell et al. 2015). Although encouraging results of Lagrangian processes (e.g., water transports and bay–ocean exchanges via tidal inlets being well simulated using the three-dimensional (3D) hydrodynamic model; surface and bottom measurements indicating distinct transport patterns over various sub-bays) in a shallow lagoonal system had been gained indirectly from numerical models and fixed-point Eulerian measurements (Kang et al. 2017; Mao and Xia 2018), new information about surface circulation patterns revealed from direct drifter observations was still lacking (Kumar et al. 2015). Hydrodynamic simulations from Mao and Xia (2018) indicate that water currents in Chincoteague Inlet are relatively weaker than those of Ocean City Inlet, yet water exchanges across the former inlet are stronger than the latter due to larger geographic dimensions. Additionally, both Kang et al. (2017) and Mao and Xia (2018) suggest that winds and tides are primarily responsible for water exchanges through the paired inlets in the Maryland Coastal Bays system (MCBs). However, both studies lack the analysis of current characteristics by direct Lagrangian observations (e.g., using surface drifters) under various wind–tide conditions. Because the flows in a shallow lagoonal system with intricate geometry and coastline are highly complex (Dever et al. 1998), analyzing a large collection of surface drifter movements over a wide spatial coverage and long-time span can provide valuable insights into coastal circulation (Schmidt et al. 2003).

Although Lagrangian observations were conducted previously in large water bodies including Lake Michigan (Mao and Xia 2020), northern Gulf of Mexico (Sun et al. 2020), and Denmark Strait (Saberi et al. 2020), investigations of water currents between an estuary and the coastal ocean were mainly conducted with numerical models and Eulerian measurements (Valle-Levinson and Lwiza 1995; Valle-Levinson et al. 1996, 2001; Salles et al. 2015). Wang et al. (2013) studied surface currents with the collection of measurements from three ADCP (acoustic Doppler current profiler) meters near Ocean City Inlet (MD), indicating that inlet circulation is primarily controlled by tides. Kang et al. (2017) simulated bay–ocean exchanges of MCBs under various wind conditions, suggesting that tidal effects on inlet circulation gradually weakened with the increasing wind intensity (e.g., > 7 m/s). However, both Wang et al. (2013) and Kang et al. (2017) lacked Lagrangian observations that directly reflect water currents with a wide spatial coverage and a long-time span. To this date, a few researchers have managed successfully to reveal the complex current patterns of the MCBs (e.g., weak circulation in the lagoon, strong currents across inlets, and alongshore movements in the coastal ocean), yet the forcing mechanism (e.g., wind effects at various tidal phases) remains partially understood and still requires further research (Beudin et al. 2017; Ganju et al. 2017).

Kang et al. (2017) provided encouraging results on the relative contributions of winds and tides to inlet circulation, but did not focus on a particular tidal phase under the synergistic effects of tides and winds. A recent study by Mao and Xia (2018) indicated that bay and inlet circulation varied significantly between the ebb and flood phases (e.g., outflow and inflow). Both studies concluded that tides dominate transports in low wind conditions, while wind-induced transport is substantial during strong wind events or hurricanes. A recent modeling study by Zhang et al. (2018) in Radial Sand Ridges (China) confirmed the strong dependence of inlet transports on wind scales. Based on an observational study, Wong and Valle-Levinson (2002) stated that winds can modify the subtidal exchange at the entrance of the Chesapeake Bay through both local and remote forces. Subsequently, Valle-Levinson et al. (2015) revealed significant effects of tidal flows on exchange processes between Choctawhatchee Estuary and Gulf of Mexico via the shallow Destin inlet (FL).

Previous studies on surface currents/transports in lagoon–inlet–coastal ocean systems were either restricted to tidal inlets or hydrodynamic models, while drifter-based studies were lacking. Consequently, surface movements have not been well characterized and quantified regarding the relative effects of winds and tides to surface movements in a lagoon–inlet–coastal ocean system by drifter observations. In MCBs, Wang et al. (2013) reported that the water quality in northern bays was relatively inferior because of locally weak and stagnant flows (Mao and Xia 2018). By analyzing a unique dataset of surface drifters, this study can potentially have broad implications to coastal oceanographers and policy makers for properly monitoring coastal water quality and creating a forward-thinking plan in similar coastal zones (e.g., estimated surface circulation pattern as an indicator of nutrient and pollutant transports and residence time). To capture the characteristics of surface currents in a lagoon–inlet–coastal ocean system, we deployed surface drifters within the inlet, in the lagoon, and at the river mouth of MCBs at various tidal phases (e.g., ebb, flood, and slack) in 2017 and 2018 (Table 1 and Fig. 1). The remaining sections are organized as follows. Methodology introduces methodology, including the study domain, background, drifter design, field campaign, and data collection. Overview of the study domain shows results of surface drifter observations under various tide and wind conditions. Discussion and conclusions are given in Background and Surface drifter design.

Methodology

Overview of the Study Domain

The Maryland Coastal Bays system (MCBs; a total area of ~282 km^2) is located behind the barrier islands of

Table 1 Information of drifter deployments including tidal phase, location, start and end times, and drifting speeds. LWL/HWL is abbreviated as low/high water level, and LWL/HWL + 1 h means 1 h after low/high water (note: the interval is set at 0.5 h for concise)

Drifter No	Tidal phase at release	Release location	Release coordinates (Long., Lat.)	Water depth at releasing (m)	Geographic feature at the release site	End location	Start time	End time	Drifter speed (cm/s)
							2017	2017	
B1D1	Ebb (HWL + 2 h)	OCI	(−75.0915°, 38.3274)	4.2	Along OCI's north shore	Coastal ocean	03/29 15:47	04/01 05:56	19
B1D2	Ebb (HWL + 2 h)	OCI	(−75.0917°, 38.3274)	4.0		Open ocean	03/29 15:55	10/20 21:46	45
B1D3	Flood (LWL + 4 h)	OCI	(−75.0905°, 38.3321)	3.8	Between OCI's north and IWB's east shores	IWB	03/29 23:44	04/01 03:58	12
B1D4	Flood (LWL + 4 h)	OCI	(−75.0918°, 38.3275)	4.0	Along OCI's north shore	Open ocean	03/29 23:48	07/11 14:46	32
B2D1	Ebb (HWL + 3 h)	OCI	(−75.0916°, 38.3250)	5.3	At OCI's deep channel	Open ocean	05/25 14:50	07/11 13:37	29
B2D2	Ebb (HWL + 3 h)	OCI	(−75.0882°, 38.3242)	4.7	In the middle part of OCI	Coastal ocean	05/25 14:54	06/16 17:20	27
B2D3	Slack before flood (LWL + 0.5 h)	OCI	(−75.0882°, 38.3242)	4.7		Coastal ocean	05/25 18:11	05/26 01:26	21
B2D4	Slack before flood (LWL + 0.5 h)	OCI	(−75.0899°, 38.3245)	4.0		Coastal ocean	05/25 18:14	05/25 23:07	17
B3D1	Slack before flood (LWL−1 h)	OCI	(−75.0905°, 38.3242)	5.5	At OCI's deep channel	Coastal ocean	06/21 14:49	06/22 19:05	20
B3D2	Slack before flood (LWL−1 h)	OCI	(−75.0866°, 38.3240)	4.8	At OCI's mouth	Coastal ocean	06/21 14:51	06/22 14:39	21
B3D3	Flood (LWL + 1 h)	OCI	(−75.0866°, 38.3238)	4.8		Coastal ocean	06/21 17:00	06/22 16:41	19
B3D4	Flood (LWL + 1 h)	OCI	(−75.0866°, 38.3238)	4.8		Coastal ocean	06/21 17:00	06/22 16:13	19
B4D1	Slack before ebb (HWL + 0.5 h)	OCI	(−75.0877°, 38.3239)	4.2	Between OCI's mouth and jettied channel	OCI	07/26 15:58	07/26 16:20	50
B4D2	Slack before ebb (HWL + 0.5 h)	OCI	(−75.0877°, 38.3239)	4.2		SB	07/26 15:58	07/26 18:11	47
B4D3	Ebb (HWL + 3.5 h)	OCI	(−75.0877°, 38.3239)	4.2		Coastal ocean	07/26 19:01	07/27 03:24	33
B4D4	Ebb (HWL + 3.5 h)	OCI	(−75.0877°, 38.3239)	4.2		OCI	07/26 19:01	07/27 04:14	30
B5D1	Slack before flood (LWL)	CI	(−75.4105°, 37.8808)	4.8	At CI's mouth and on the east side of the deep channel	Coastal ocean	09/30 14:08	10/04 16:26	14
B5D2	Flood (LWL + 6.5 h)	CI	(−75.4105°, 37.8774)	3.2		Coastal ocean	09/30 20:21	10/03 22:16	13
B5D3	Flood (LWL + 6.5 h)	CI	(−75.4112°, 37.8764)	2.9		Coastal ocean	09/30 20:15	10/04 00:30	13
B5D4	Flood (LWL + 6.5 h)	CI	(−75.4064°, 37.8741)	3.2		Coastal ocean	09/30 20:26	10/04 00:12	11
B6D1	Ebb (HWL + 3 h)	OCI	(−75.0587°, 38.3234)	6.0	At OCI's mouth	SB	10/20 15:45	10/20 23:45	11

Table 1 (continued)

Drifter No	Tidal phase at release	Release location	Release coordinates (Long., Lat.)	Water depth at releasing (m)	Geographic feature at the release site	End location	Start time	End time	Drifter speed (cm/s)
B6D2	Ebb (HWL+3 h)	IWB	(−75.0936°, 38.3720)	1.9	In the middle part of IWB	Coastal ocean	10/20 15:59	10/22 23:49	13
B6D3	Ebb (HWL+2 h)	CB	(−75.2538°, 38.1067)	2.1	In the middle part of CB	CB	10/20 14:48	10/24 10:41	9
B6D4	Ebb (HWL+3.5 h)	OCI	(−75.0875°, 38.3238)	4.4	Between OCI's mouth and jettied channel	Coastal ocean	10/20 16:20	10/22 02:06	17
							2018	2018	
B7D1	Ebb (HWL+3.5 h)	AB	(−75.0894°, 38.4006)	2.0	In the southern AB	IWB	05/28 15:10	05/29 15:42	11
B7D2	Flood (LWL+2.5 h)	IWB	(−75.1000°, 38.3579)	1.8	Along IWB's south shore	IWB	05/28 20:16	05/29 11:09	10
B7D3	Ebb (HWL+4.5 h)	SB	(−75.1334°, 38.2829)	1.6	In the middle part of SB	SB	05/28 16:12	05/28 19:06	54
B7D4	Ebb (HWL+5 h)	CB	(−75.2139°, 38.1884)	1.3	In the northern CB	CB	05/28 16:47	05/30 22:56	7
B8D1	Ebb (HWL+4 h)	OCI	(−75.0882°, 38.3239)	4.2	Between OCI's mouth and jettied channel	Coastal ocean	06/26 15:12	06/26 22:11	36
B8D2	Ebb (HWL+4.5 h)	SMR	(−75.1167°, 38.3834)	1.7	At the mouth of SMR	IWB	06/26 15:40	06/28 21:50	6
B8D3	Ebb (HWL+5 h)	SMR	(−75.1828°, 38.4133)	0.9	In the upstream of SMR	SMR	06/26 16:05	06/28 15:12	2
B8D4	Ebb (HWL+5.5 h)	OCI	(−75.0893°, 38.3246)	4.4	In the middle part of OCI	Coastal ocean	06/26 16:48	06/26 21:19	19
B9D1	Ebb (HWL+4 h)	OCI	(−75.0881°, 38.3238)	4.2	Between OCI's mouth and jettied channel	Coastal ocean	07/12 15:20	07/12 20:42	28
B9D2	Ebb (HWL+4.5 h)	SMR	(−75.1185°, 38.3839)	1.8	At the mouth of SMR	IWB	07/12 15:52	07/12 21:07	8
B9D3	Ebb (HWL+3.5 h)	IWB	(−75.1255°, 38.3765)	1.6	Along IWB's west shore	IWB	07/14 04:51	07/14 22:12	11

Fenwick and Assateague and adjacent to Delmarva Peninsula of the U.S. East Coast (Fig. 1a). It comprises five backbays and multiple tributaries (Boynton et al. 1996; Wazniak et al. 2005): Assawoman Bay (AB), Isle of Wight Bay (IWB), Sinepuxent Bay (SB), Newport Bay (NB), Chincoteague Bay (CB), and St. Martin River (SMR). Tidal exchanges with the coastal ocean are restricted to a pair of microtidal inlets, namely Ocean City Inlet (OCI) to the north and Chincoteague Inlet (CI) to the south (Fig. 1b, c).

Flushing rates are inversely related to the distance from the adjacent inlet (Pritchard 1960; Thomas et al. 2009). The low flushing rates facilitate the long-term retention of nutrients, sediments, and contaminants. The MCBs includes shallow shoals in the lagoon and deep channels in the inlets (e.g., 0.5–3- and 4–8 m water depths, respectively). Widths of OCI range from 160 m at its seaward edge to 330 m in the middle, while they reach 2 km for CI. The limited inlet's width restricts its exchange with the adjacent coastal ocean.
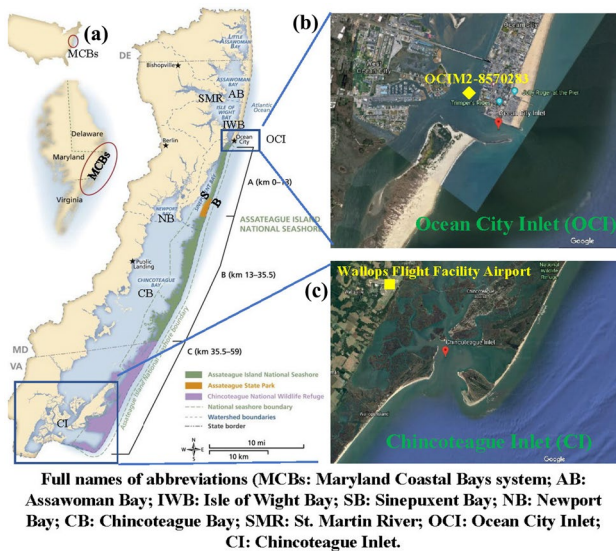
Full names of abbreviations (MCBs: Maryland Coastal Bays system; AB: Assawoman Bay; IWB: Isle of Wight Bay; SB: Sinepuxent Bay; NB: Newport Bay; CB: Chincoteague Bay; SMR: St. Martin River; OCI: Ocean City Inlet; CI: Chincoteague Inlet.

Fig. 1 **a** Maps of Maryland Coastal Bays system adjusted from Wazniak et al. (2005) and aerial images of **b** Ocean City Inlet and **c** Chincoteague Inlet from Google Earth

Background

The MCBs provides shelters for numerous fish, shellfish, and wildlife species and supports the recovery of blue crab, finfish, hard clam, and oyster fisheries, which contributes $1–3 billion annually to the States of Delaware, Maryland, and Virginia (Martin et al. 2018). However, increased anthropogenic pressures, continuous land development, and agricultural activities pose major threats to estuarine health (Wazniak et al. 2004). As a result of low flushing rates and limited tidal exchanges (Boynton et al. 1996), this lagoonal system is highly vulnerable to eutrophication (Bricker et al. 1999). Excessive nutrients in the water column enable the formation of harmful algal blooms, resulting in localized hypoxic conditions harmful to fish and wildlife (Hall and Wazniak 2005). Although pollutants entering the MCBs tend to remain within the bays (Wazniak et al. 2005), they can contribute to oceanic pollution via advective transports across tidal inlets (Dennison et al. 2016). To better predict pathways and fates of the passively transporting materials, an enhanced understanding of water currents in the MCBs is necessary. Amplitudes of the dominated lunar semidiurnal M2 tide along the seaward coast near OCI, IWB, AB, and CB are 1–1.3, 0.5–0.9, 0.3–0.5, and 0.1–0.3 m (Wang et al. 2013). Tidal currents entering the MCBs via OCI are strong (e.g., up to 2.6 m/s) during the flood phase, of which 85% moves into IWB and AB (U.S. Army Corps of Engineers 1998). Water currents on the inner continental shelf outside the MCBs move southward, while their directions occasionally reverse in April and September when the prolonged
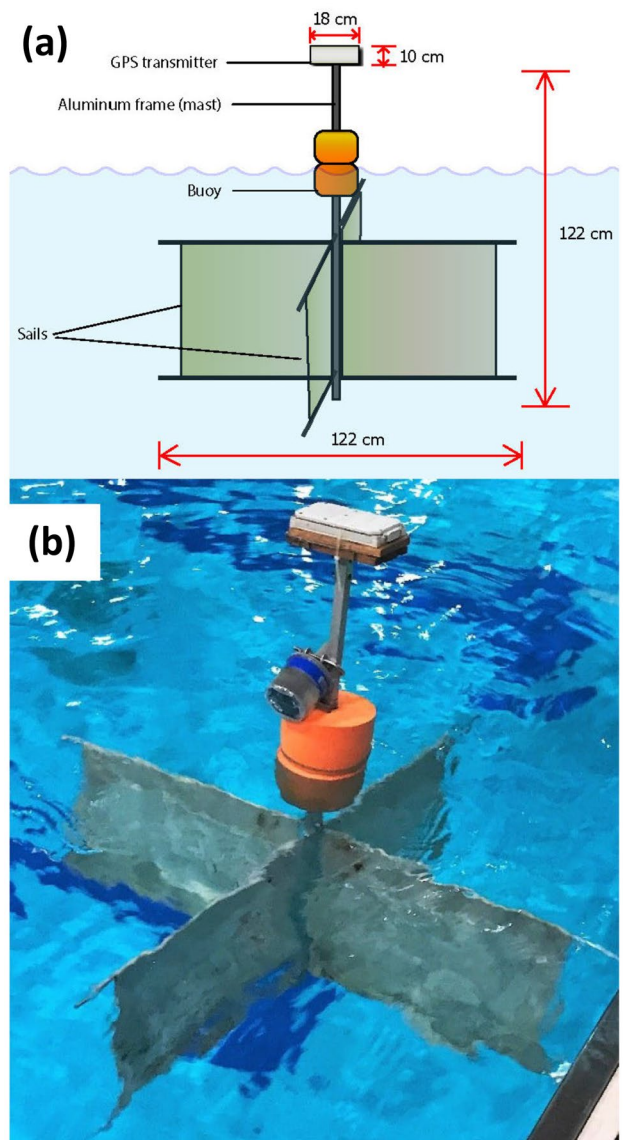
southerly winds dominate. The jetties constructed near OCI disrupt the nearshore flow between Ocean City and Assateague Island, potentially resulting in an accelerated degradation of the Assateague shoreline (Rosati and Ebersole 1996).
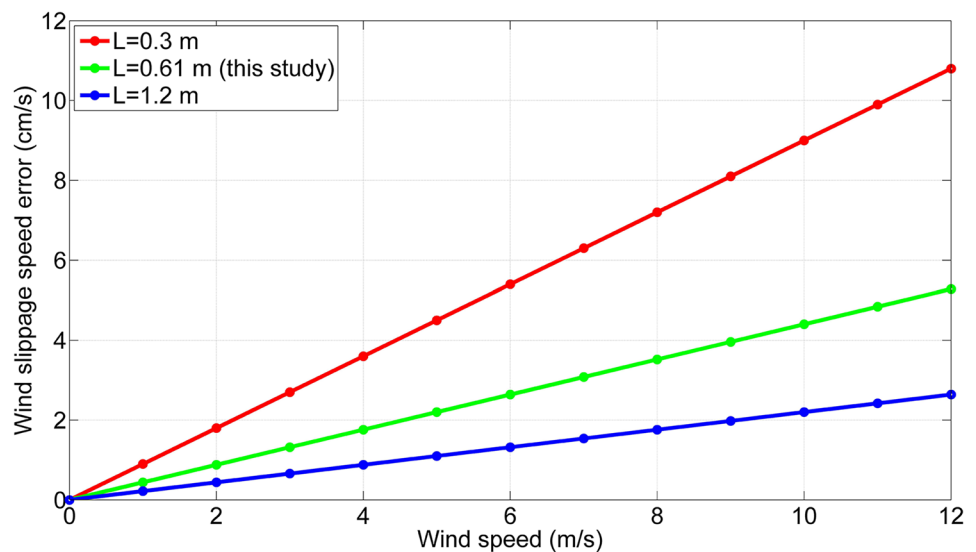
Surface Drifter Design

Surface drifters are built and assembled according to the cruciform-shaped Irina design (Pelletier et al. 2017), a low-cost version of the Coastal Ocean Dynamics (CODE) drifter (Davis 1985). To effectively follow surface currents, avoid running aground, and lessen the direct wind effects, the height of surface drifters is reduced in the shallow MCBs

Fig. 2 **a** Components and dimensions of the modified Irina drifter; **b** a surface drifter was tested in a swimming pool

(Fig. 2). Each surface drifter consists of a square aluminum tube to support the GPS (global positioning system) transmitter, a subsurface drogue with four canvas cloth vanes and aluminum spars, a GPS transmitter mounted to pine woods, two stacked foam buoys, and a sleeve through each mast. The subsurface drogue extends 0.5 m below the water surface. A Satellite Transmitter Integrated GPS Receiver is housed in a waterproof case fastened to the wooden mount. The receiver operates over the Globalstar Simplex data network that transmits the drifter's coordinate position. To ensure visibility, a solar-powered marine strobe is fastened to the mast above the buoy with a U-bolt. To offset the weight of the strobe and U-bolt (~0.45 kg) and to maintain a stable buoyancy, two Mountain Security 40-mm Long Shackle Laminated Steel Padlocks ($91 \times 25 \times 142$ mm and 0.24 kg for each) are attached to the bottom spars with carabiner clips. To accurately represent surface flows by drifters, the wind slippage effect was minimized by reducing the drogue length properly (Fig. 3). Estimations of the windage error u_0 at a specific wind speed W are based on Murray (1975):

$$u_0 = \left(\frac{C_2 \sigma D h \sin\theta}{C_1 \rho} \right)^{\frac{1}{2}} \frac{W}{L} \tag{1}$$

where C_1 and C_2 are drag coefficients of the drogue (1.2) and circular pole (1.0); σ and ρ are the air and water densities (1.29 and 1.0×10^3 kg/m^3); D and h are the diameter of the pole (0.05 m) and its exposed length (0.52 m); L is the length of a side of the drogue (0.61 m in this study); and θ is the tilt angle of the line to the vertical (15 °). Then, Eq. (1) simplifies to $u_0 = 0.44 \times 10^{-2} W$. Even at a high wind speed (e.g., 12 m/s), the windage effect is ~5 cm/s, which is negligible in most cases compared with the wind-induced surface currents in the MCBs (Mao and Xia 2018). CODE-type drifters have been widely used in coastal ocean applications.

Field Campaign, Data Collection, and Skill Metrics

During 2017–2018, 35 surface drifters (25 in the inlets and 10 in the lagoon) were released and collected in nine field campaigns (Table 1). Percentages of drifter data are 60%, 34%, and 6% ending up in the coastal/open ocean, lagoon, and inlet, respectively. Although many surface drifters ended up in the coastal/open ocean, most of them have passed through the paired inlets in the middle of tidal transitions. Coordinate positions of drifters were transmitted every 2 h for the deployments in March and May 2017, which were gradually reduced to 1 or 0.5 h in the remaining experiments. Based on the preliminary data analysis, it was found that higher sampling frequency can reflect the true trajectories more accurately (e.g., the analyzed path connecting adjacent locations may pass through land if the sampling resolution is overly low). On the premise of ensuring sufficient battery level, the sampling resolution was changed from two hours to half an hour. Each surface drifter was assigned to an identification number based on the deployment time and order (e.g., B1D1 means that the surface drifter was in the first batch and released in the first deployment). The mean distance, speed, and direction of surface currents were derived from the recording time of signal transmission and GPS coordinates. Given that the number of drifter tracks passing over land only occupies a tiny percentage of the total drifter observations, the mean distance of each drifter is calculated linearly between two points. Hourly wind data collected at OCIM2–8,570,283 (38.328°N, 75.091°W) and Wallops Flight Facility Airport (37.937°N, 75.467°W) were operated by the NOAA's National Data Buoy Center and the National Centers for Environmental Information, respectively. Hourly tide data near OCI were collected from NOAA's OCIM2–8,570,283 station at (38.328°N, 75.091°W). It should be noted that the tidal gauge is near OCI and might

Fig. 3 Estimations of windage errors for the rectangular cross-sectional drogues with various lengths of a side of the drogue based on the formulation of Murray (1975)

not be representative of the water level elsewhere (e.g., the southern part of the lagoon) due to tidal wave deformation. Thus, the phase difference of tides should be considered as a factor when analyzing the relationship between water-level variations and drifter movements.

The dependence of surface drifter velocities on winds and tides was evaluated using the Person correlation coefficient (*CC*), which was expressed as follows:

$$CC = \frac{\sum_{m=1}^{M} \sum_{n=1}^{N} (x_{mn} - \overline{x})(y_{mn} - \overline{y})}{\sqrt{\left(\sum_{m=1}^{M} \sum_{n=1}^{N} (x_{mn} - \overline{x})^2\right)\left(\sum_{m=1}^{M} \sum_{n=1}^{N} (y_{mn} - \overline{y})^2\right)}} \quad (2)$$

where $\overline{x}$ and $\overline{y}$ are the mean values of the data sets x_{mn} and y_{mn}, respectively, in a sample of size M. N refers to the dimension of the sample, and $N = 1$ and 2 are used for one-dimensional (1D) scalar (e.g., tidal ranges) and two-dimensional (2D) vector (e.g., wind speed), respectively. *CC* measures linear correlations between wind speeds (tidal levels) and surface drifter velocities in the 2D (1D) space. The absolute values of *CC*, which are in the ranges of 0–0.3, 0.3–0.5, 0.5–0.7, and 0.7–1, indicate little/no, weak, moderate, and strong linear associations, respectively. When the drifter records are long enough and the p-value of the calculated *CC* is less than 0.05, these tests are considered statistically significant. Because some correlations have too little pairs to be meaningful, a 95% confidence interval (i.e., alpha = 0.05) for *CC* is computed as well.

Results

Surface Drifters Released at the Ebb Phase Near Ocean City Inlet

To investigate tidal and wind effects, surface drifters were categorized according to various tidal phases and releasing locations (Table 1). B1D1, B1D2, B2D1, B2D2, B4D3, B4D4, B6D1, B6D4, B8D1, B8D4, and B9D1 started their movements at the ebb phase near Ocean City Inlet (OCI). B1D1 deployed on March 29, 2017, moved into the coastal ocean and back to OCI during the flood tide. In 3 d, it drifted into the adjacent coastal ocean and then became stranded on the shore of Assateague Island (Fig. 4a). B1D2 followed a similar path initially, but then drifted into the Atlantic Ocean for more than half a year (Fig. 4b). The magnitudes of northwesterly winds from April 1 to 2 were 6–10 m/s, and during this time, B1D2 exhibited a southward movement along the shoreline at speeds of 10–46 cm/s (Fig. 5a). Between April 3 and 5, winds switched to a southwesterly direction with speeds of 3–10 m/s, during which B1D2 exhibited a northward and longshore drifter movement at 44 cm/s. B2D1 and B2D2 deployed on May 25,
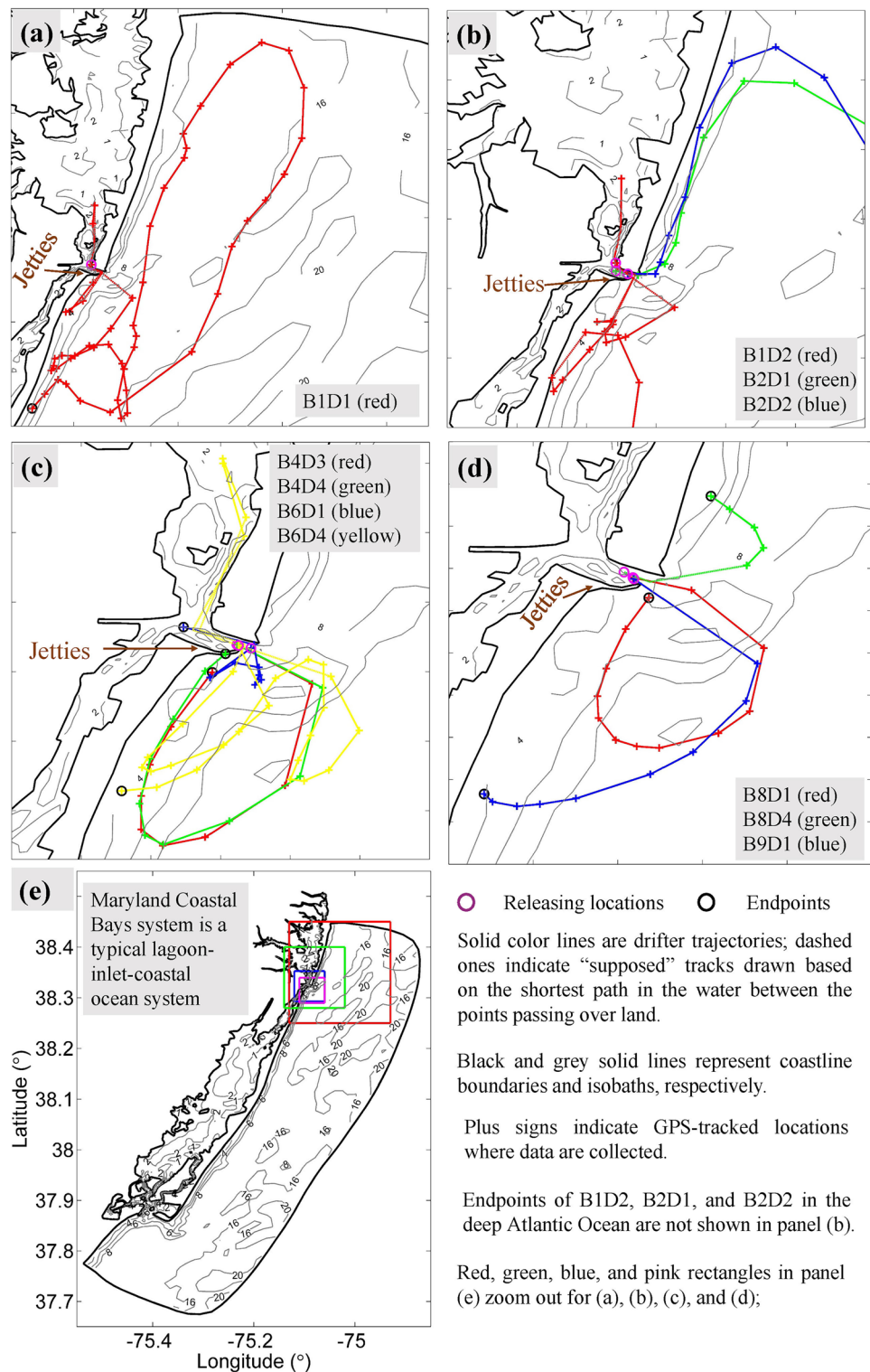
2017, immediately moved into the coastal ocean, followed by northward and longshore movements. The westerly wind on May 26 reached 9 m/s (Fig. 5b), preceding a southeastward drifter movement into the coastal ocean (Fig. 4b). B4D3 and B4D4 were deployed on July 26, 2017 (Fig. 4c), and moved into the coastal ocean at a 1-km distance from the inlet mouth. As the tide phase shifted from ebb to flood coinciding with easterly weak winds of 2–4 m/s (Fig. 5d), surface drifters moved in a clockwise direction before running aground on the southern jetty. Surface drifter movements from OCI to the coastal ocean reveal an ebb tidal flow extending from its mouth to the coastal ocean at a length scale of 1.5 km, forming a clockwise and circular movement. Similar trajectories between B4D3 and B4D4 demonstrate the high stability of surface drifters to represent surface flows. B6D1 deployed on October 20, 2017, started at the seaward edge of OCI, where B6D4 was released 35 min later. During the drifting period, the magnitude of the northeasterly wind was 4.2 m/s (Fig. 5f), and B6D4 exhibited northwesterly movements shifting in a clockwise direction modulated by the M2 tide. Over an 8 h period following its deployment, B6D1 exited OCI to Assateague Island and back to the inlet by following the flood tide (Fig. 5f). The distant paths between B6D1 and B6D4 suggest that trajectories of surface drifters vary according to their release times under shifting wind conditions and tidal phases.

In 2018, B8D1/B8D4 and B9D1 were deployed at the mouth of OCI on June 26 and July 12, respectively. Southeasterly winds with magnitudes of 2–6 m/s prevailed on June 26 (Fig. 5h), while both B8D1 and B8D4 traveled in an opposite direction relative to this mild local wind during the ebb tide phase. B8D4 exited OCI and ran aground on Fenwick Island within 5 h, while B8D1 traveled in a clockwise direction before it ran aground on the south jetty of OCI. B9D1 entered the coastal ocean in a clockwise direction at the ebb phase, similar to the initial path of B8D1. Coinciding with an easterly wind with a magnitude of 3.6 m/s, it moved westward and ran aground on Assateague Island in 5 h. B8D1 and B9D1 exhibited a similar movement initially (e.g., opposite to the wind direction) while showing distinct paths subsequently. Taking B9D1 as an example, its trajectory generally followed the cycle of ebb and flood currents (e.g., offshore and onshore movements) on July 12, during which the westward component of the wind speed was 3.48 m/s. Its pathway showed a southward directional shift following a southward component of local winds with a magnitude of 0.93 m/s.

Surface Drifters Released at Non-ebb Tide Phases Near Ocean City Inlet

B1D3 and B1D4 started movements on March 29, 2017, at the flood phase near OCI (Fig. 6a, b). Wind speeds between March 29 and April 1 ranged from 3 to 12 m/s, and their directions

Fig. 4 **a–d** Trajectories for the surface drifters released at the ebb phase near Ocean City Inlet and **e** domain of Maryland Coastal Bays system. Time periods of drifter trajectories are listed in Table 1. Based on the isobath map, deep channels, and shoals at the middle of the inlet and near the shallow coast in the lagoon, respectively

currents are strong near OCI and along the channel of IWB. In the following stages, B1D3 ran aground on an island in IWB, while B1D4 entered the Atlantic Ocean. B3D3 and B3D4 deployed on the outer edge of OCI at the flood phase on June 21, 2017, moved northward along the coast, and ran aground on

varied from northeasterly, easterly, and southeasterly (Fig. 5a). Despite the wind effect, both surface drifters moved northward into Isle of Wight Bay (IWB) during the flood currents. This phenomenon is supported by previous studies from Kang et al. (2017) and Mao and Xia (2018), which stated that flood

Fig. 5 Time series of the observed drifter velocity, elevation, and wind speed during nine batches of drifting period. Red and blue solid lines represent the west–east and south–north components of drifter velocities or wind speeds, respectively
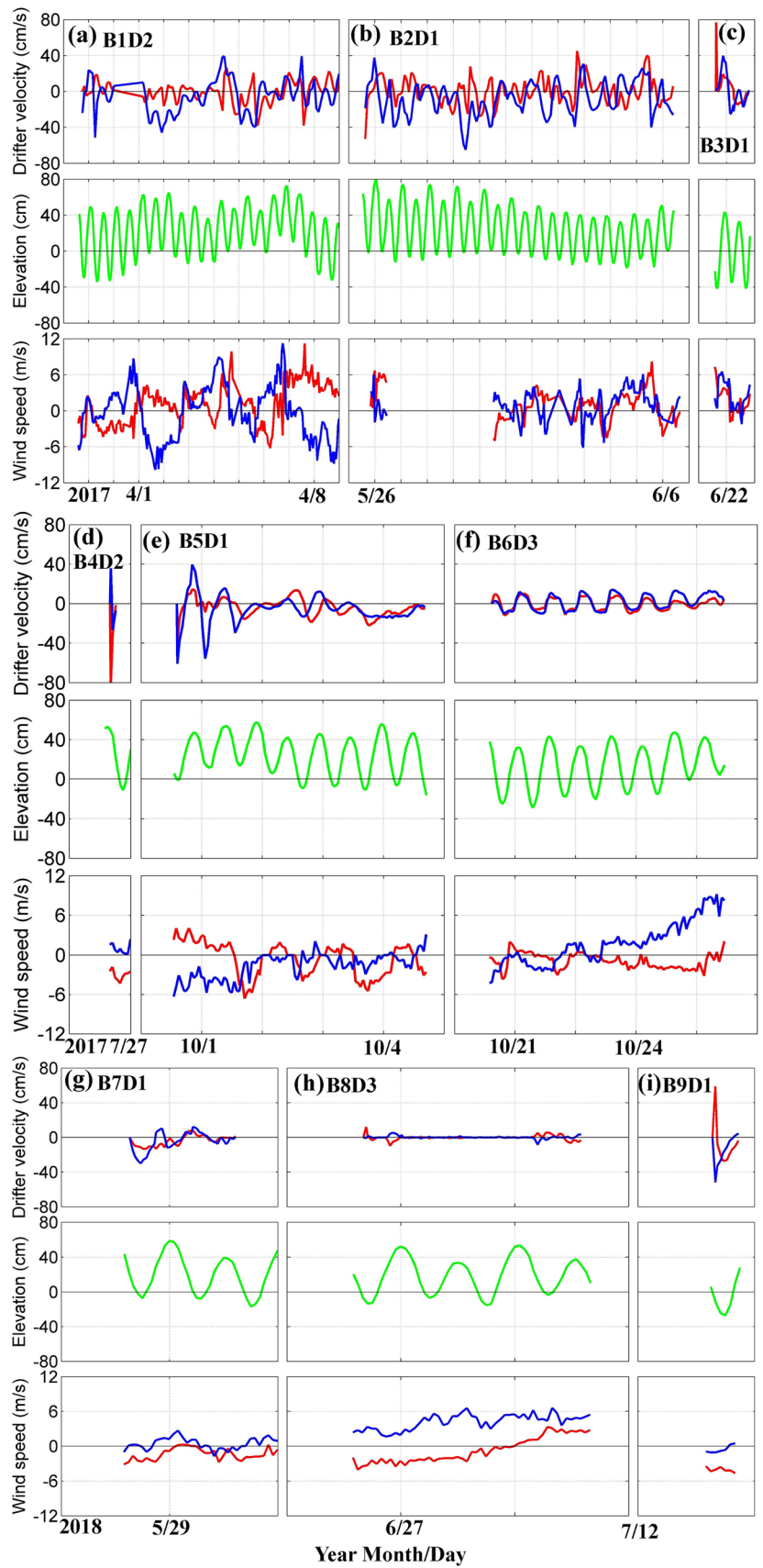
Fig. 6 Trajectories for the surface drifters released at **a–b** flood, **c** slack before flood, and **d** slack before ebb phases near Ocean City Inlet; **e** domain of Maryland Coastal Bays system. Time periods of drifter trajectories are listed in Table 1. Based on the isobath map, deep channels, and shoals at the middle of the inlet and near the shallow coast in the lagoon, respectively
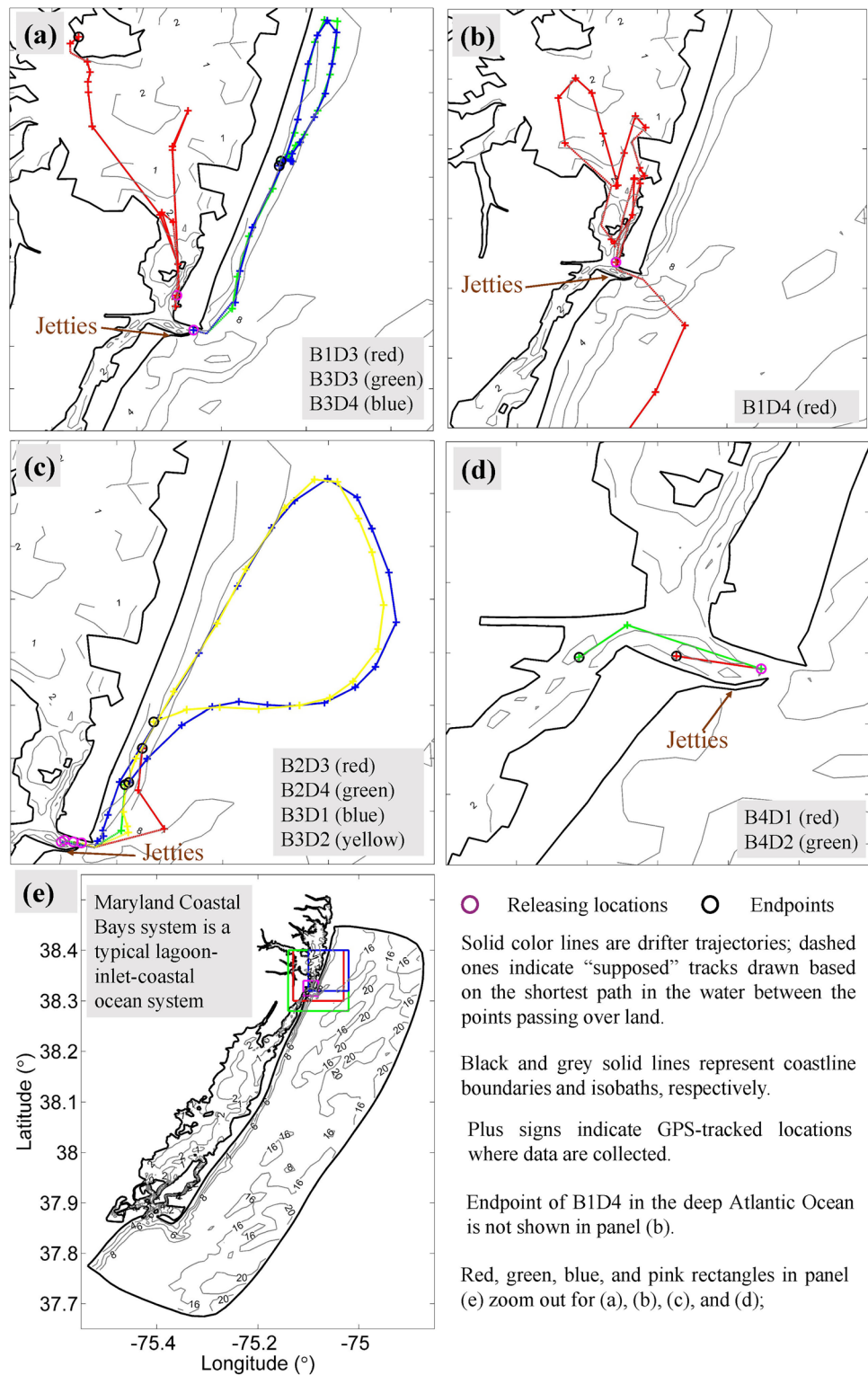
Fenwick Island (Fig. 6a). These movements are different from those of B1D3, indicating that drifter trajectories are highly sensitive to initial releasing locations (e.g., outer edge versus inner OCI) and wind conditions (e.g., westerly winds at 7.6 m/s during the third batch).

Although B3D1 and B3D2 were released at the same location as that of B3D3 and B3D4, the former drifters started at the slack phase before flood and thus showed relatively weak movements along the shore while stronger and offshore activities (e.g., moving away from the shore

initially and coming back in a clockwise direction). As the wind direction switched from southwesterly to southeasterly at speeds of 4 m/s in 14 h after its release (Fig. 5c), pronounced onshore movements were observed for both drifters (Fig. 6c). B2D3 and B2D4 were released on May 25, 2017, at the slack before flood phase. Although the southwesterly and westerly winds led to an initially offshore movement for B2D3 and B2D4, they moved northward and closer to shore before becoming stranded on Fenwick Island during the flood tide. B4D1 and B4D2 deployed in OCI at the slack phase before ebb on July 26, 2017, traveled through OCI and ran aground shortly in SB (Fig. 6d). Tidal currents were quite weak at the slack phase, and during this time, easterly/southeasterly winds ranged from 1.8 to 4.4 m/s.

Surface Drifters Released Near Chincoteague Inlet and Backbays

The surface drifters released in the fifth batch started movements on September 30, 2017, at the (slack before) flood phase near Chincoteague Inlet (CI) (Fig. 7a). During the following period of this deployment, the strong northerly wind was up to 6.7 m/s and B5D1 moved southward into the coastal ocean at the slack before flood phase. During the following flood and ebb phases, it moved northward into the inlet and then southward to the coastal ocean. The other drifters moved northward initially, followed by the southward movement into the coastal ocean during the ebb tide. All drifters continued moving southward and ran aground on Metompkin Islands, VA (75°34'W, 38°44'N), at 18–21 km distances to the inlet mouth nearby in 3 d. The fastest surface drifting speed was in the middle of CI at 72 cm/s. It can be concluded that tidal currents are primarily responsible for surface drifter movements when winds are weak, and increased wind intensities are important for surface drifters approaching the shore. B6D3 was deployed in the middle of Chincoteague Bay (CB) at the ebb phase on October 20, 2017 (Fig. 7d) and exhibited a southward movement upon its release. During this time, northerly winds prevailed at speeds of 4.2 m/s. The drifter switched its directions following each tidal phase shift, with speeds under 15 cm/s until it ran aground on the west bank of CB. During the transit of B7D4, easterly winds prevailed with speeds under 3.3 m/s. This drifter exhibited back-and-forth movements before running aground in CB, similar to those of B6D3.

B6D2 deployed on October 20, 2017, at the ebb phase in IWB moved out of OCI under the synergistic effects of northeasterly winds and ebb currents (Fig. 7b). During the following flood and ebb tides, it drifted to IWB before moving back to the coastal ocean. Driven by the southeasterly winds on the October 22 (Fig. 5f), it traveled onshore to Assateague Island. On May 28, 2018, B7D1 and B7D2 were deployed at the ebb phase in Assawoman Bay (AB) and

flood phase in IWB, respectively (Fig. 7b), when the easterly winds were mild (e.g., below 4.5 m/s) (Fig. 5j). B7D1 traveled southwestward into IWB and ran aground on the western bank, while B7D2 moved back and forth for 15 h at the northern end of OCI. B9D3 deployed in IWB at the ebb phase on July 14, 2018, showed a southward movement during the ebb tide. Because B9D3 was closer to the adjacent OCI, its drifting speed was greater than that of B7D1 (e.g., 43 cm/s along the channel of IWB versus below 32 cm/s). Because tidal currents in SB with a narrow channel were strong (Mao and Xia 2018), B7D3 was primarily driven by ebb currents. During its transit, B7D3 moved toward OCI with drifting speeds up to 71 cm/s. B8D2, B8D3, and B9D2 were deployed at the ebb phase in St. Martin River (SMR) (Fig. 7c), where tidal currents were weak (e.g., below 10 cm/s in the upper stream, see Mao and Xia 2018). Their surface drifter paths mainly followed the directions of the wind-driven surface currents (e.g., southeasterly and easterly for the eighth and ninth batches, respectively).

Discussion

Surface Drifter Trajectories in the Lagoon and Coastal Ocean

By analyzing the observed surface drifter movements, surface circulation patterns were investigated in various regions of Maryland Coastal Bays system (MCBs). Overall, most drifters entered the coastal ocean through the paired inlets during the ebb tide, except for B3D3 and B3D4 during the flood tide. This exception occurred when strong westerly winds reached 7.6 m/s. A total of 17 surface drifters entered and then remained in the ocean (e.g., 11, 4, and 2 released at the ebb, slack, and flood phases), 2 entered the ocean and moved back to the lagoon, 4 entered the ocean, back to the lagoon and then to the ocean again, and 12 never left the lagoon (e.g., in backbays away from the adjacent inlet).

After entering the lagoon via OCI, four (two) surface drifters moved northward (southward) into IWB (SB). Surface drifters that entered the lagoon from the coastal ocean through CI mainly stayed within the inlet before being carried back into the coastal ocean during the following ebb tide. Two surface drifters released in CB ran aground on its western flank; one released in AB traveled southwestward into IWB during the ebb tide; one released in IWB was aground on its western bank during the flood tide; another one released in SB ran aground at the entrance of OCI at the ebb tide. For the one released near SMR at the ebb tide ran aground nearby, and another released in Bishopville Prong at the ebb tide remained within the tributary. The finding that flow patterns in MCBs and the coastal ocean are dominated by tides under mild wind conditions (e.g., less than 7 m/s)

Fig. 7 Trajectories for the surface drifters released at **a** Chincoteague Inlet, **b** Assawoman Bay and Isle of Wight Bay, **c** St. Martin River, **d** Sinepuxent Bay and Chincoteague Bay; **e** domain of Maryland Coastal Bays system. Time periods of drifter trajectories are listed in Table 1. Based on the isobath map, deep channels, and shoals at the middle of the inlet and near the shallow coast in the lagoon, respectively
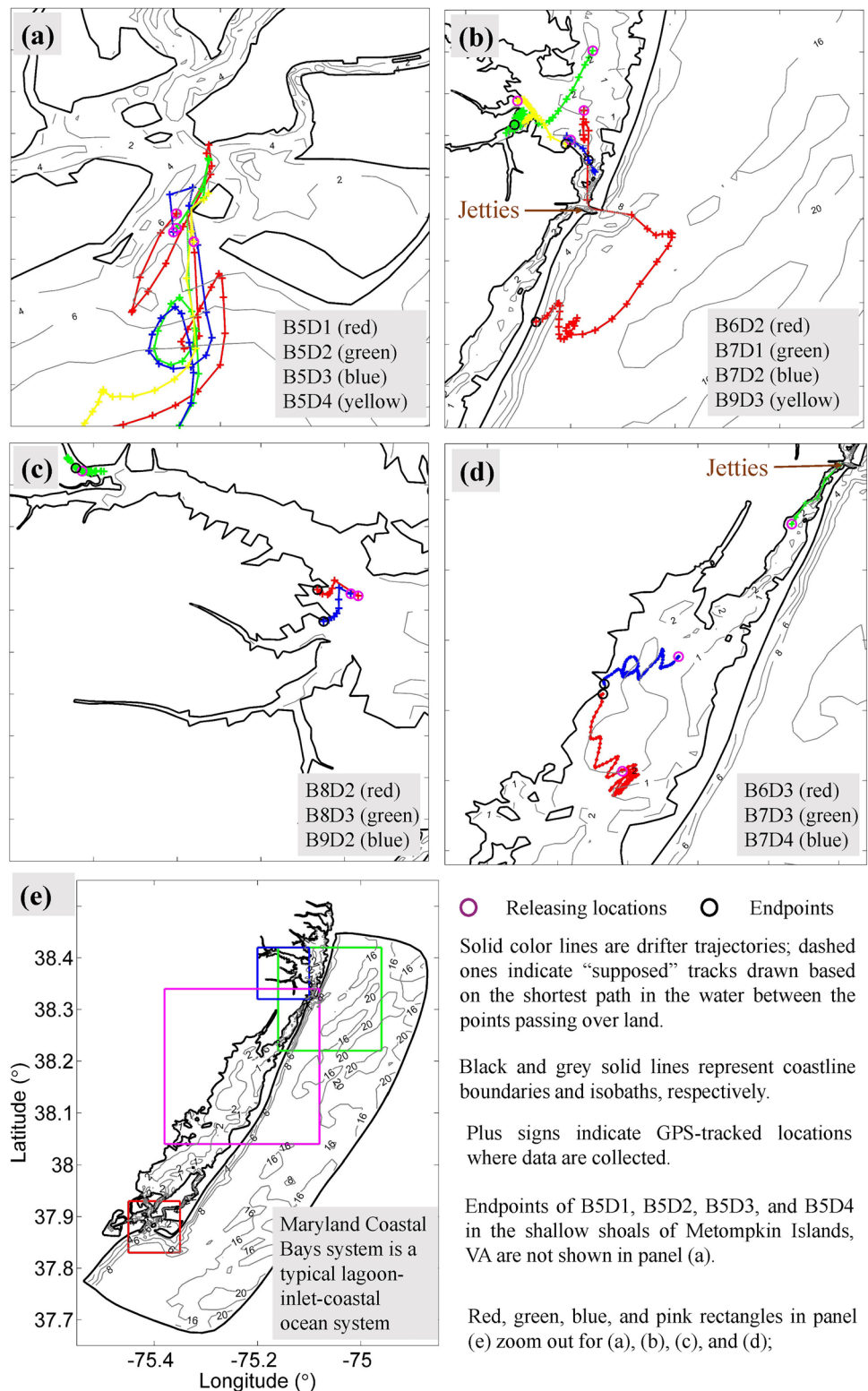
is supported by Kang et al. (2017). Under strong wind conditions (e.g., over 7 m/s), surface drifter trajectories (e.g., B3D3 and B3D4) show an obvious longshore movement, consistent with previous findings (U.S. Army Corps of Engineers 1998; Kang et al. 2017; Mao and Xia 2018). At the mouth of OCI, an ebbing jet was indicated by drifter trajectories in the summer of 2017 and 2018 (e.g., B4D3 and B4D4) under mild wind conditions (e.g., less than 6 m/s).

Table 2 Mean speeds and standard deviations of drifters in various regions of Maryland Coastal Bays system

| Regions	Number of observations	Mean drifter speed (cm/s)	Standard Deviation (cm/s)
CB	185	8.2	3.5
CI	19	34.8	15.7
IWB	129	11.3	13.3
IWB tributaries	122	3.3	3.5
OCI	11	77.2	29.3
SB	7	45.3	20.3

The large areal extent of the offshore and cross-shelf surface transports reflected by drifter trajectories released in the first two batches indicates that materials originating from coastal regions can reach Atlantic Ocean (Dennison et al. 2016). This conclusion has significant implications for pollutants and debris found in the deep ocean, implying that coastal microplastics can potentially contribute to the global ocean via water currents (Zhang 2017; Zhao et al. 2019). Therefore, it would be a worthwhile effort to continue monitoring surface flows both in the coastal regions and open ocean with additional surface drifters.

Spatial Variability of Surface Drifter Speeds

Overall, the fastest surface drifter speed was recorded in OCI (e.g., 77 cm/s), but lowest in IWB tributaries (e.g., 3 cm/s in Table 2). This finding is useful to evaluate the exchanging ability between the lagoon and coastal ocean via this tidal inlet, and the potential use of tidal current turbines for renewable energy generation in this region (Muller et al. 2016). In Fig. 8, four outliers in IWB represented accelerated surface drifter speeds near OCI (e.g., 43, 46, 53,

and 83 cm/s), the outlier in SB at 7 cm/s reflected the surface drifting speed before being aground, and the outlier in CI at 72 cm/s showed the maximum surface speed within the inlet. To determine whether a significant difference of surface drifter speeds was presented across six regions of MCBs, one-way ANOVA Tukey HSD (Tukey honest significant differences) multiple pairwise comparisons were conducted with a p-value at 0.005. It was found that variations of surface drifter speeds between IWB and CB and those between SB and CI were insignificant (e.g., p-values of 0.06 and 0.13, respectively). Further analysis showed that higher surface speeds were primarily near OCI, followed by SB, CI, IWB, CB, and IWB. Low surface speeds in IWB tributaries including Bishopville Prong have implications for the local water quality. Previous field observations and model simulations reveal hypoxia in the upstream region of SMR, associated with the elevated algae concentrations (Wang et al. 2013). Degraded water quality with excessive nutrients and organic materials in upper bays is presumably caused by locally weak flows (Mao and Xia 2018) or slow movements of surface drifters.

The dataset of drifter trajectories is consequent and could be further used as the basis of a pertinent research. For instance, since most drifters are released at OCI (followed by CI), a comparison of water exchanges between the paired inlets under various wind-tide conditions can be conducted based on the derived Lagrangian velocities. Based on the applied hydrodynamic model at MCBs (Mao and Xia 2018), the widths (and mean depths) at the mouth of OCI and CI are 0.2 and 1 km (and 4.5 and 4.4 m), respectively. Given that the mean current velocity across OCI and CI is 0.78 and 0.35 m/s (Fig. 8), respectively, the estimated water exchanges accordingly are 702 and 1540 m^3/s. The Lagrangian drifter observations support the numerical study of Mao and Xia (2018), which states that water exchanges across CI are greater than OCI due to a larger width of the

Fig. 8 Box plots of the drifter-derived current speeds in various backbays of MCBs
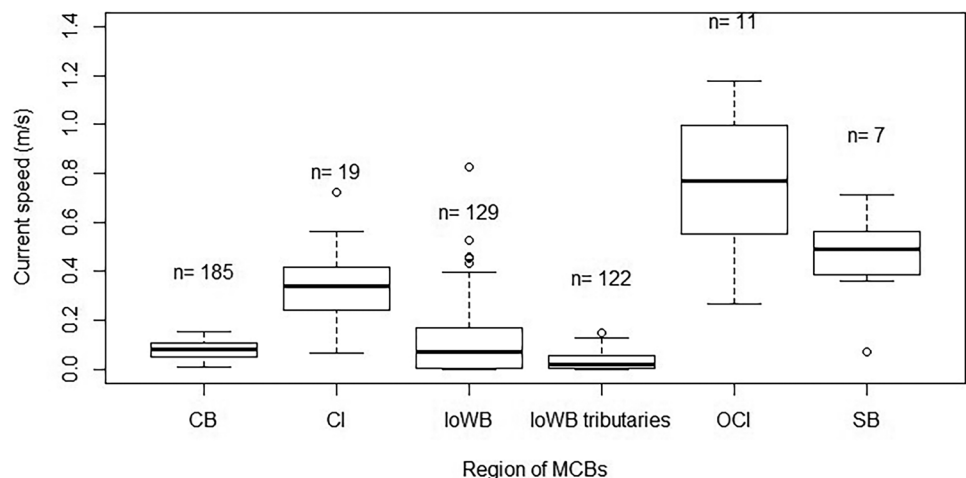
inlet mouth. The water exchanges estimated under normal wind conditions are smaller than that during Hurricane Irene (2011), for instance, 702 and 1540 m^3/s versus 1888 and 4933 m^3/s across OCI and CI (Mao and Xia 2018). The significant influence of the extreme wind intensity on bay–ocean transport is supported in the Barnegat Bay during Hurricane Sandy (2012) (Defne et al. 2019). Our observational study is a preliminary description of the water circulation in a lagoon–inlet–coastal ocean system, and future study will focus on a narrow and well-identified research question by including particle-tracking models under extreme weather conditions (Dobbelaere et al. 2022). Future endeavor would be worthwhile to validate the numerical model with additional Lagrangian measurements and explore the bay–ocean exchanges during hurricane events/winter storms using a coupled observation–modeling system.

Relative Effects of Tidal Ranges and Wind Speeds on Surface Drifters

The ability of these surface drifter trajectories in representing surface currents and transport of passive particles (or actual objects) has been proved satisfactorily off the Northern California coast during the Coast Dynamics Experiments (CODE) (Davis 1985), in the Gulf of Mexico during the Grand Lagrangian Deployment (GLAD) (Jacobs et al. 2014) and Lake Michigan on the nearshore–offshore dynamics (Mao and Xia 2020). Given that tides and winds are two major forces driving surface currents that further force surface drifters to move in the same direction accordingly, relative effects of tidal ranges and wind speeds on surface drifter movements were investigated in this subsection.

Based on the included angle between the wind speed and drifting velocity, movements of surface drifters relative to winds were categorized into strongly following, weakly following, strongly opposing, and weakly opposing (e.g., 0–45°, 45–90°, 90–135°, 135–180°). Figure 9 shows the relationships between surface drifters and wind directions under various tide-wind conditions. At weak winds with speeds ≤ 3 m/s (e.g., left sides of the gray dashed lines in Fig. 9a, b), tidal forcing is the major driver of the surface drifter movement near OCI (e.g., the percentages of drifter data are 33% and 22% in the strongly and weakly opposing directions of winds, respectively). This finding agrees with that of Kang et al. (2017), which stated the stronger dependence of the exchanging ability on tides as winds became weaker via the northern tidal inlet of MCBs. By contrast, both winds and tides are important to surface drifter dynamics near CI and backbays even under weak wind conditions with speeds ≤ 3 m/s (e.g., the percentages of drifter data are 39% and 32% in the strongly and weakly following directions of winds, respectively, see Fig. 9c, d). This is due to larger geographic sizes than OCI, which facilitated the

development of long-fetch winds and thus greater wind-induced surface currents and Lagrangian movements (Mao and Heron 2008). Driven by the increasing wind, drifter movements gradually became stronger. When the magnitude of winds > 10 m/s, surface drifters generally showed strongly/weakly following movements (Fig. 9a, b). Due to the bottom friction-induced dissipation (Mao and Xia 2018), the required least wind speed of following movements decreased to 6.4 m/s in the shallow backbays (Fig. 9c, d).

To further investigate the relationship between wind speeds (tidal levels) and surface drifter velocities, the corresponding Pearson correlation coefficients (CC) were calculated (Table 3). Drifters released in the third batch showed moderate to strong associations with wind speed vectors (e.g., CC in the range of 0.66–0.7) under strong wind conditions (7.6 m/s). For the CC between tidal levels and surface drifter velocities, a moderate association was found for B6D1 (e.g., $CC = 0.68$) by following the ebb and flood cycles (e.g., moving into the coastal ocean and back to the lagoon via OCI). Under weak wind conditions (e.g., wind speed ≤ 3.56 m/s), there was little/no (e.g., $CC = -0.19$) association between this drifter's velocity and wind speed.

In this study, ebb (flood) is defined as the tidal phase during which the water level is falling (rising). For tidal inlet systems, the ebb (flood) current corresponds to seaward (landward) flow. In addition, phase variations are influenced by the variation of spatial locations where observations are taken. Consequently, there are phase lags/leads between water levels and surface drifter movements (e.g., ebb/flood current reverses after the highest/lowest water levels). Based on the cross-correlation function, the phase difference between water levels observed in IWB and surface drifter velocities recorded in the coastal ocean outside CI was a 5-h forward for B5D1.

Study Limitation

It should be mentioned that surface drifter movements are very random, and their trajectories and endpoints can be distinct under certain circumstances, yet they are released at the same time and location (Gough et al. 2019; Aksamit et al. 2019; Spydell et al. 2021). This is because Lagrangian errors accumulate quickly over time (Liu et al. 2011). Particle trajectories are highly complex and sensitive to initial conditions, but the surface currents in the system are relatively robust by forming a wall or passage for material transports, which become the Lagrangian coherent structure (LCSs) of the flow (Haller 2015).

Analysis of surface drifter observations could bring new information about the bay–ocean exchanges and validate the particle-tracking model (Liu et al. 2014), which cannot come directly from fixed-point measurements. Although this preliminary investigation provides insight into the characteristics of drifter movements under various wind–tide
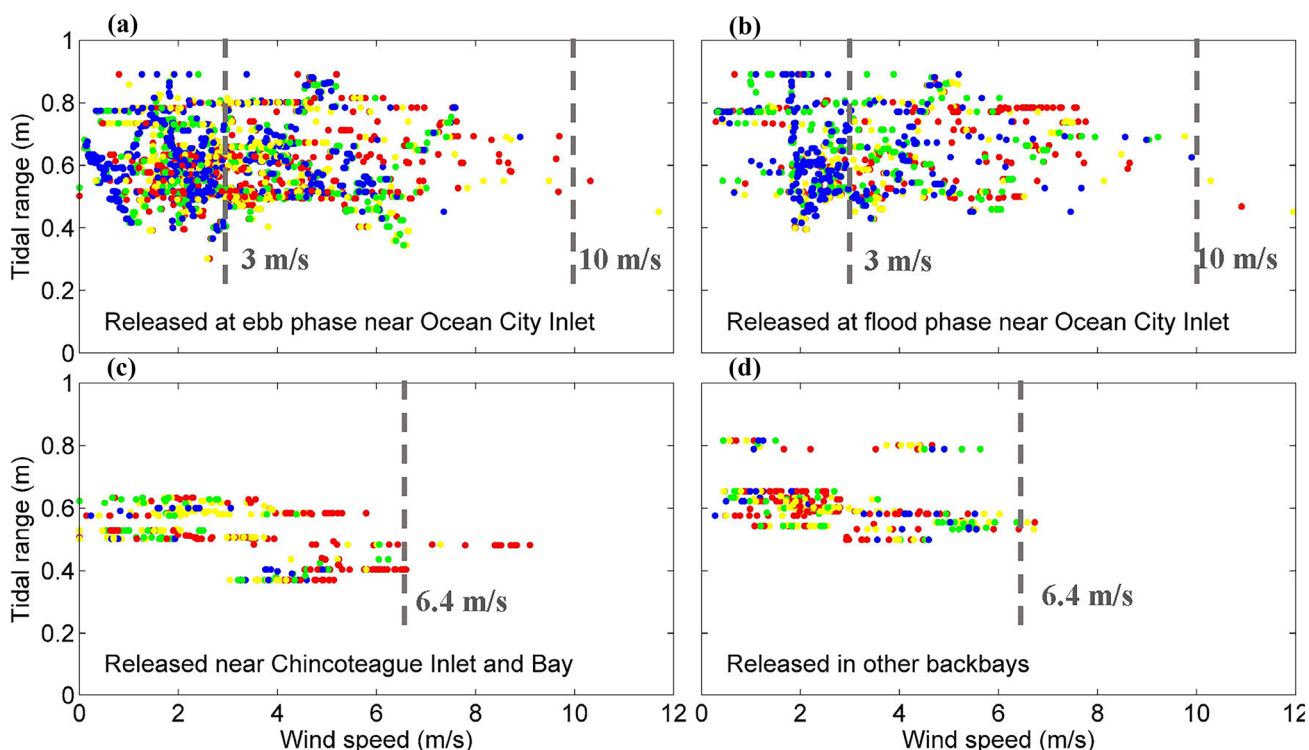
The colored dots represent the relationship of directions (θ) between drifter velocity and wind speed
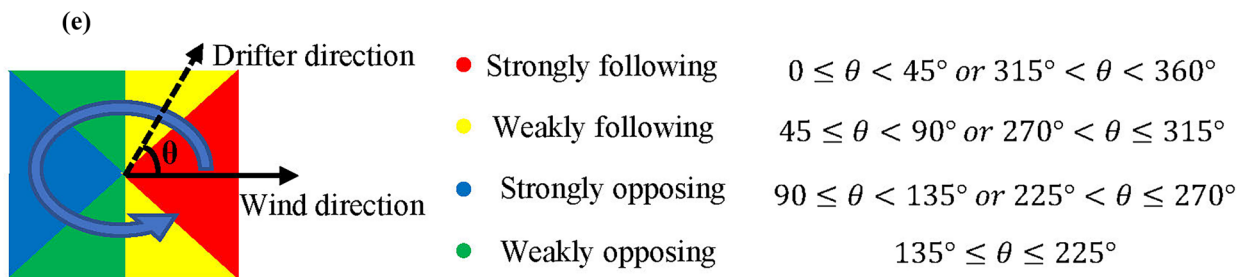
Fig. 9 Relationships between drifter and wind directions under various tide–wind conditions for drifters released at **a** ebb and **b** flood phases near Ocean City Inlet, **c** Chincoteague Inlet and Bay, and **d** other backbays based on the definition in diagram **e**. The specified wind speeds mentioned in the content are indicated with gray dashed lines in panels **a**–**d**

conditions, observations are restricted to 2D space (e.g., visualizing a small component of the 3D circulation with surface information in a semi-enclosed basin). Even if the water column is mixed, wind-driven flows may be vertically sheared with opposite directions in the surface and bottom layers. Thus, this rudimentary work can be potentially useful to further study the degraded water quality (e.g., surface drifters move slowly in a small region) for the extremely shallow and well-mixing water bodies, of which the vertical variability of horizontal currents is quite weak. During the analysis of surface drifter trajectories, we find that some of the data points lead to their traveling paths over land due to the low temporal resolution of drifter position (e.g., near OCI where surface flows are intense). To comprehensively analyze

the 3D structures of water masses (e.g., hypoxia water) and flow properties, it is worthwhile in future to apply drifters with drogues being applied at various water depths (Rypina et al. 2021), coordinate positions being recorded at a higher temporal resolution (Spydell et al. 2015), advanced algorithms (e.g., finite time/space Lyapunov exponent) in calculating the LCSs (Bettencourt et al. 2015), and 3D hydrodynamic–particle trajectory coupled modeling system (Mao and Xia 2020). It is expected that, with the development of the LCSs theory, drifter observation methods, and improved skill assessment scores of numerical models (e.g., normalized Lagrangian separation method, see Liu and Weisberg 2011), the complex 3D current structures and exchanging flows will be revealed better in a comprehensive way.

Table 3 Calculated correlation coefficient scores between wind speeds (CC_w) or tidal levels (CC_t) and surface drifter velocities. The CC scores calculated from long data records and that are statistically significant (i.e., p-value < 0.05), are highlighted by superscript asterisks. The lower and upper bounds for a 95% confidence interval (i.e., Alpha = 0.05) for CC_w (CC_w) are computed and expressed as CC_{wl} and CC_{wu} (CC_{tl} and CC_{tu}), respectively

Drifter No	Effective sample size M	CC_w	CC_{wl}	CC_{wu}	CC_t	CC_{tl}	CC_{tu}
B1D1	54	0.53*	0.38	0.65	0.28*	0.01	0.51
B1D2	2228	−0.05*	−0.08	−0.02	0.02	−0.03	0.06
B1D3	19	0.37*	0.06	0.62	0.31	−0.16	0.67
B1D4	1167	0.02	−0.02	0.06	−0.01	−0.07	0.05
B2D1	563	0.08*	0.02	0.14	−0.14*	−0.22	−0.05
B2D2	142	0.41*	0.30	0.50	−0.26*	−0.40	−0.10
B2D3	4	−0.33	−0.84	0.49	−0.81	−1.00	0.69
B2D4	3	−0.46	−0.93	0.56	−0.86	/	/
B3D1	29	0.66*	0.49	0.79	0.20	−0.18	0.53
B3D2	24	0.66*	0.47	0.80	0.34	−0.07	0.66
B3D3	24	0.68*	0.49	0.01	0.10	−0.32	0.48
B3D4	23	0.70*	0.51	0.82	0.05	−0.37	0.45
B4D1	1	1.00	/	/	1.00	1.00	1.00
B4D2	3	0.43	−0.59	0.92	0.93	/	/
B4D3	9	−0.13	−0.56	0.36	−0.40	−0.84	0.36
B4D4	10	−0.09	−0.51	0.37	−0.46	−0.84	0.24
B5D1	99	0.28*	0.15	0.41	−0.16	−0.35	0.03
B5D2	74	0.46*	0.32	0.58	−0.01	−0.24	0.22
B5D3	76	0.48*	0.35	0.60	0.01	−0.21	0.24
B5D4	76	0.38*	0.23	0.50	−0.15	−0.37	0.08
B6D1	8	−0.19	−0.63	0.34	0.68	−0.04	0.94
B6D2	55	0.33*	0.15	0.49	−0.37*	−0.58	−0.11
B6D3	92	0.38*	0.25	0.50	0.22*	0.02	0.41
B6D4	31	0.38*	0.15	0.58	−0.10	−0.44	0.26
B7D1	42	0.23*	0.02	0.42	−0.35*	−0.59	−0.05
B7D2	12	0.07	−0.34	0.46	−0.07	−0.62	0.52
B7D3	5	0.32	−0.38	0.79	−0.39	−0.95	0.75
B7D4	93	0.46*	0.34	0.57	−0.03	−0.24	0.17
B8D1	13	−0.13	−0.49	0.28	0.16	−0.43	0.65
B8D2	10	0.40	−0.05	0.72	−0.58	−0.88	0.08
B8D3	78	0.04	−0.12	0.20	−0.02	−0.24	0.21
B8D4	8	−0.04	−0.52	0.47	−0.52	−0.90	0.29
B9D1	9	−0.06	−0.51	0.42	−0.46	−0.86	0.30
B9D2	9	0.06	−0.42	0..51	−0.70*	−0.93	−0.07
B9D3	25	−0.25	−0.50	0.03	−0.56*	−0.78	−0.21

Conclusions

This study examined characteristics of surface currents across various regions of Maryland Coastal Bays system (MCBs) by releasing a total of 35 surface drifters at various wind–tide conditions in 2017 and 2018. Additionally, observations from local wind buoys, tide gauges, and surface drifter trajectories were analyzed. At flood phase, surface drifters likely move northward into Isle of Wight Bay after entering Ocean City Inlet (OCI). At ebb phase, drifters follow clockwise and circular movements at the outer edge of OCI. Based on the surface drifter observations and analyses, the main conclusions are summarized as follows:

1. Under weak wind conditions (e.g., ≤ 3 m/s), tides are primarily responsible for surface drifter movements near OCI, whereas both winds and tides are important to surface drifter movements near Chincoteague Inlet (CI) and in the lagoon. It adds insight to a similar system that a larger geographical dimension facilitates longer wind fetch, greater wind-induced surface currents, and drifter movements. Under strong wind conditions (e.g., > 10 m/s), surface drifter movements generally follow wind directions. In a shallow lagoon, relative effects of winds on surface drifters become stronger in the regions away from the adjacent inlet (e.g., tides are weaker).

2. Overall, surface drifters exit (enter) the lagoon mostly during ebb (flood) currents. Additionally, the fastest surface drifters are near the small OCI, and slower movements are in the lagoon due to the weakened tidal effect. Direct drifter observations of Lagrangian movements cover a wide space and long-time span in MCBs, providing a strong support to numerical simulations of a lagoon–inlet–coastal ocean system. It is a worthwhile effort to improve the design of these low-cost drifters (e.g., reflecting surface, middle, and bottom movements), as a significant supplement tool for Eulerian measurements and three-dimensional hydrodynamic model. In future, developing an observation–modeling system of MCBs can provide new insight into the exchanging characteristics and 3D circulation for coastal environments.

References

Aksamit, N.O., T. Sapsis, and G. Haller. 2019. Machine-learning mesoscale and submesoscale surface dynamics from Lagrangian ocean drifter trajectories. *Journal of Physical Oceanography* 50 (5): 1179–1196.

Annika, P., T. George, P. George, N. Konstantinos, D. Costas, and C. Koutitas. 2001. The Poseidon operational tool for the prediction of floating pollutant transport. *Marine Pollution Bulletin* 43 (7–12): 270–278.

Bettencourt, J., C. López, E. Hernández-García, I. Montes, J. Sudre, B. Dewitte, A. Paulmier, and V. Garçon. 2015. Boundaries of the Peruvian oxygen minimum zone shaped by coherent mesoscale dynamics. *Nature Geoscience* 8: 937–940.

Beudin, A., N.K. Ganju, Z. Defne, and A.L. Aretxabaleta. 2017. Physical response of a back-barrier estuary to a post-tropical cyclone. *Journal of Geophysical Research* 122: 5888–5904.

Boynton, W.R., L. Murray, J.D. Hagy, C. Stokes, and W.M. Kemp. 1996. A comparative analysis of eutrophication patterns in a temperate coastal lagoon. *Estuaries* 19 (2): 408–421.

Bricker, S.B., C.G. Clement, D.E. Pirhalla, S.P. Orlando, and D.R.G. Farrow. 1999. National estuarine eutrophication assessment: effect of nutrient enrichment in the nation's estuaries. National Oceanic and Atmospheric Administration, National Ocean Service, Special Projects Office and the National Centers for Coastal Ocean Science, Silver Spring, Maryland, USA.

Brown, C.A., G.A. Jackson, and D.A. Brooks. 2000. Particle transport through a narrow tidal inlet due to tidal forcing and implications for larval transport. *Journal of Geophysical Research* 105 (C10): 24141–24156.

Cipriani, L.E., and G.W. Stone. 2001. Net longshore sediment transport and textural changes in beach sediments along the southwest Alabama and Mississippi barrier islands, U.S.A. *Journal of Coastal Research* 17 (2): 443–458.

Davis, R.E. 1985. Drifter observations of coastal surface currents during CODE: The method and descriptive view. *Journal of Geophysical Research* 93: 4741–4755.

Defne, Z., N.K. Ganju, and J.M. Moriarty. 2019. Hydrodynamic and morphologic response of a back-barrier estuary to an extratropical storm. *Journal of Geophysical Research: Oceans* 124 (11): 7700–7717.

Dennison, W.C., C.E. Wazniak, R.V. Jesien, K.A. Phillips, C. McCollough, R.B. Sturgis, R.H. Kelsey, and J.E. Thomas. 2016. *Maryland Coastal Bays 2016: Land and bay perspectives*, 28. Cambridge, MD: IAN Press.

Dever, E.P., M.C. Hendershott, and C.D. Winant. 1998. Statistical aspects of surface drifter observations of circulation in the Santa Barbara Channel. *Journal of Geophysical Research* 103 (C11): 24781–24797.

Dobbelaere, T., M. Curcic, M. Le Hénaff, and E. Hanert. 2022. Impacts of Hurricane Irma (2017) on wave-induced ocean transport processes. *Ocean Modelling* 171: 101947.

Ganju, N.K., S.E. Suttles, A. Beudin, D.J. Nowacki, J.L. Miselis, and B.D. Andrews. 2017. Quantification of storm-induced bathymetric change in a back-barrier estuary. *Estuaries and Coasts* 40: 22–36.

Gough, M.K., F.J. Beron-Vera, M.J. Olascoaga, J. Sheinbaum, J. Jouanno, and R. Duran. 2019. Persistent Lagrangian transport patterns in the northwestern Gulf of Mexico. *Journal of Physical Oceanography* 49 (2): 353–367.

Hall, M., and C. Wazniak. 2005. Continuous water quality monitoring in the Maryland Coastal Bays: 2004 annual report. Maryland Department of Natural Resources, Annapolis, Maryland, USA.

Haller, G. 2015. Lagrangian coherent structures. *Annual Review of Marine Science* 47: 137–162.

Harrington, M.W. 1894. *Currents of the Great Lakes: As deduced from the movements of bottle papers during the seasons of 1982 and 1983*. Washington, D.C.: U.S. Weather Bureau.

Jacobs, G.A., et al. 2014. Data assimilation considerations for improved ocean predictability during the Gulf of Mexico Grand Lagrangian Deployment. *Ocean Modelling* 83: 98–117.

Jenkins, G.P., K.P. Black, M.J. Wheatley, and D.N. Hatton. 1997. Temporal and spatial variability in recruitment of a temperate, seagrass-associated fish is largely determined by physical processes in the pre- and post-settlement phases. *Marine Ecology Progress Series* 148: 23–35.

Kang, X., M. Xia, J.S. Pitula, and P. Chigbu. 2017. Dynamics of water and salt exchange at Maryland Coastal Bays. *Estuarine, Coastal and Shelf Science.* 189: 1–16.

Kjellsson, J., and K. Döös. 2012. Surface drifters and model trajectories in the Baltic Sea. *Boreal Environment Research* 17: 447–459.

Krafft, D. 2017. Drifter study of circulation near Indian River Inlet, DE (Master thesis). University of Delaware. http://udspace.udel.edu/handle/19716/23095, accessed April 2022.

Kumar, N., F. Feddersen, Y. Uchiyama, J. McWilliams, and W. O'Reilly. 2015. Mid-shelf to surf zone coupled ROMS-SWAN model-data comparison of waves, currents, and temperature: Diagnosis of subtidal forcings and response. *Journal of Physical Oceanography.* 45: 1464–1490.

Liu, Y., and R.H. Weisberg. 2011. Evaluation of trajectory modeling in different dynamic regions using normalized cumulative Lagrangian separation. *Journal of Geophysical Research: Oceans* 116: C09013.

Liu, Y., R.H. Weisberg, C. Hu, and L. Zheng. 2011. Tracking the Deepwater Horizon oil spill: A modeling perspective. *EOS, Transactions, American Geophysical Union* 92 (6): 45–46.

Liu, Y., R.H. Weisberg, S. Vignudelli, and G.T. Mitchum. 2014. Evaluation of altimetry-derived surface current products using Lagrangian drifter trajectories in the eastern Gulf of Mexico. *Journal of Geophysical Research: Oceans* 119: 2827–2842.

Lumpkin, R., T. Özgökmen, and L. Centurioni. 2017. Advances in the application of surface drifters. *Annual Review of Marine Science* 9: 59–81.

Mao, M., and M. Xia. 2018. Wave-current dynamics and interactions near the two inlets of a shallow lagoon-inlet-coastal ocean system under hurricane conditions. *Ocean Modelling* 129: 124–144.

Mao, M., and M. Xia. 2020. Particle dynamics in the nearshore of Lake Michigan revealed by an observation-modeling system. *Journal of Geophysical Research: Oceans* 125: e2019JC0157654.

Mao, Y., and M.L. Heron. 2008. The influence of fetch and the response of surface currents to wind studies by HF ocean surface radar. *Journal of Physical Oceanography* 38 (5): 1107–1121.

Martin, J., J. Young, G.J. Kauffman, and A. Homsey. 2018. Economic value of the Maryland Coastal Bays watershed. Retrieved from Maryland Coastal Bays Program. https://mdcoastalbays.org/coastal-bays-economic-report-review, retrieved March 2021.

McNally, G.J. 1981. Satellite-tracked drift buoy observations of the near-surface flow in the Eastern mid-latitude North Pacific. *Journal of Geophysical Research* 86 (C9): 8022–8030.

Molcard, A., L.I. Piterbarg, A. Griffa, T.M. Özgökmen, and A.J. Mariano. 2003. Assimilation of drifter observations for the reconstruction of the Eulerian circulation field. *Journal of Geophysical Research* 108 (C3): 3056.

Muller, M.W., Z. Rue, and K. Hiebler. 2016. Investigation of the potential use of tidal current turbines in the Ocean City, Maryland inlet for renewable energy generation. *Smart Grid and Renewable Energy* 7: 142–146.

Murray, S.P. 1975. Trajectories and speeds of wind-driven currents near the coast. *Journal of Physical Oceanography* 5: 347–360.

Norcross, B.L., and R.F. Shaw. 1984. Oceanic and estuarine transport of fish eggs and larvae: A review. *Transactions of the American Fisheries Society.* 113 (2): 153–165.

Pelletier, E., C. Stymiest, and J. Manning. 2017. Student Drifter Construction Manual 2017. https://studentdrifters.org/wp-content/uploads/2017/10/Drifter-Manual_10052.017.pdf, accessed April 2022.

Pritchard, D.W. 1960. Salt balance and exchange rate for Chincoteague Bay. *Chesapeake Science.* 1 (1): 48–57.

Reed, M., C. Turner, and A. Odulo. 1994. The role of wind and emulsification in modelling oil spill and surface drifter trajectories. *Spill Science & Technology Bulletin* 1 (2): 143–157.

Rosati, J.D., and B.A. Ebersole. 1996. Littoral impact of Ocean City Inlet, Maryland, USA, in Coastal Engineering 1996: Proceedings of the Twenty-Fifth International Conference, September 2–6, 1996, edited by B. L. Edge, pp. 2779– 2792, American Society of Civil Engineering, New York.

Rypina, I.I., T.R. Getscher, L.J. Pratt, and B. Mourre. 2021. Observing and quantifying ocean flow properties using drifters with drogues at different depths. *Journal of Physical Oceanography* 51 (8): 2463–2482.

Saberi, A., T.W.N. Haine, and R. Gelderloos. 2020. Lagrangian perspective on the origins of Denmark Strait Overflow. *Journal of Physical Oceanography* 50 (8): 2393–2414.

Salles, P., A. Valle-Levinson, A. Sottolichio, and N. Senechal. 2015. Wind-driven modifications to the residual circulation in an ebb-tidal delta: Arcachon Lagoon, Southwestern France. *Journal of Geophysical Research: Oceans* 120: 728–740.

Schmidt, W.E., B.T. Woodward, K.S. Millikan, R.T. Guza, B. Raubenheimer, and S. Elgar. 2003. A GPS-tracked surf zone drifter. *Journal of Atmospheric and Oceanic Technology* 20: 1069–1075.

Spydell, M.S., F. Feddersen, and J. Macmahan. 2021. Relative dispersion on the inner shelf: Evidence of a Batchelor regime. *Journal of Physical Oceanography* 51 (2): 519–536.

Spydell, M.S., F. Feddersen, M. Olabarrieta, J. Chen, R.T. Guza, B. Raubenheimer, and S. Elgar. 2015. Observed and modeled drifters at a tidal inlet. *Journal of Geophysical Research* 120: 4825–4844.

Sun, D., A. Bracco, R. Barkan, M. Berta, D. Dauhajre, M.J. Molemaker, J. Choi, G. Liu, A. Griffa, and J.C. McWilliams. 2020. Diurnal cycling of submesoscale dynamics: Lagrangian implications in drifter observations and model simulations of the northern Gulf of Mexico. *Journal of Physical Oceanography* 50 (6): 1605–1623.

Thomas, J.E., J.L. Woerner, D.P. Blazer, M.L. Luckenbach, M.L. Tarnowski, C.E. Wazniak, and D.E. Wilson. 2009. Chincoteague Bay. pp. 138—148. Cultural change in Maryland's Coastal Bays.

Turrell, W.R. 1994. Modelling the Braer oil spill – A retrospective view. *Marine Pollution Bulletin* 28 (4): 211–218.

U.S. Army Corps of Engineers. 1998. Ocean City, Maryland and vicinity water resources study: Final feasibility report and environmental impact statement with appendices. U.S. Army Corps of Engineers, Baltimore District. https://mdcoastalbays.org/files/pdfs_pdf/ocean-city-final-feasibility-report-and-EIS_Part1.pdf, accessed March 2021.

U.S. Coast Guard. 2013. U.S. Coast Guard addendum to the United States National Search and Rescue Supplement (NSS) to the International Aeronautical and Maritime Search and Rescue Manual (IAMSAR). Command. Instr. M16130.2F, US Coast Guard, US Department of Homeland Security, Washington, DC.

Valle-Levinson, A., and K.M.M. Lwiza. 1995. The effects of channels and shoals on exchange between the Chesapeake Bay and the adjacent ocean. *Journal of Geophysical Research: Oceans* 100 (C9): 18551–18563.

Valle-Levinson, A., J.M. Klinck, and G.H. Wheless. 1996. Inflows/outflows at the transition between a coastal plain estuary and the coastal ocean. *Continental Shelf Research* 16 (14): 1819–1847.

Valle-Levinson, A., K. Huguenard, L. Ross, J. Branyon, J. MacMahan, and A. Reniers. 2015. Tidal and nontidal exchange at a subtropical inlet: Destin Inlet, Northwest Florida. *Estuarine, Coastal and Shelf Science* 155: 137–147.

Valle-Levinson, A., K.C. Wong, and K.T. Bosley. 2001. Observations of the wind-induced exchange at the entrance to Chesapeake Bay. *Journal of Marine Research* 59 (3): 391–416.

Wang, H., Z. Wang, J.D. Loftis, and Y.C. Teng. 2013. Hydrodynamic and water quality modeling and TMDL development for Maryland's coastal Bays system. Final report submitted to Maryland Department of the Environment, TMDL Technical Development Program.

Wazniak, C., M. Hall, C. Cain, D. Wilson, R. Jesien, J. Thomas, T. Carruthers, and W. Dennison. 2004. State of the Maryland coastal bays. Maryland Department of Natural Resources, Maryland Coastal Bays Program, and University of Maryland Center for Environmental Science, College Park, Maryland.

Wazniak, C., D. Wells, and M. Hall. 2005. The Maryland coastal bays ecosystem. Document number: DNR-12–1202–0009. pp. 1–20. In: Wazniak, C.E., Hall, M.R. (Eds.), Maryland's Coastal Bays: Ecosystem Health Assessment 2004. Maryland Department of Natural Resources, Annapolis, MD.

Wong, K.C., and A. Valle-Levinson. 2002. On the relative importance of the remote and local wind effects on the subtidal exchange at the entrance to the Chesapeake Bay. *Journal of Marine Research* 60 (3): 477–498.

Xia, M., L. Xie, and L.J. Pietrafesa. 2007. Modeling of the Cape Fear River estuary plume. *Estuaries and Coasts* 30 (4): 698–709.

Xia, M., L. Xie, and L.J. Pietrafesa. 2010. Winds and the orientation of a coastal plane estuary plume. *Geophysical Research Letters* 37: L19601.

Xia, M., L. Xie, L.J. Pitrafesa, and M.M. Whiteney. 2011. The ideal response of a Gulf of Mexico estuary plume to wind forcing: Its connection with salt flux and a Lagrangian view. *Journal of Geophysical Research* 116: C08035.

Zhang, H. 2017. Transport of microplastics in coastal seas. *Estuarine, Coastal and Shelf Science* 199: 74–86.

Zhang, W.N., H.M. Huang, Y.G. Wang, D.K. Chen, and L. Zhang. 2018. Mechanistic drifting forecast model for a small semi-submersible drifter under tide-wind-wave conditions. *China Ocean Engineering* 32 (1): 99–109.

Zhao, S., T. Wang, L. Zhu, P. Xu, X. Wang, L. Gao, and D. Li. 2019. Analysis of suspended microplastics in the Changjiang Estuary: Implications for riverine plastic load to the ocean. *Water Research* 161: 560–569.